Journal of Alloys and Compounds 478 (2009) 83–88

Contents lists available at ScienceDirect

Journal of Alloys and Compounds

journal homepage: www.elsevier.com/locate/jallcom

Electrocrystallization of Pb and Pb assisted Al on aluminum electrode from molten salt ($AlCl_3$–NaCl–KCl)

M. Jafarian [a,*], I. Danaee [a], A. Maleki [a], F. Gobal [b], M.G. Mahjani [a]

[a] Department of Chemistry, K.N. Toosi University of Technology, P.O. Box 15875-4416, Tehran, Iran
[b] Department of Chemistry, Sharif University of Technology, P.O. Box 11365-9516, Tehran, Iran

ARTICLE INFO

Article history:
Received 2 September 2008
Received in revised form
25 November 2008
Accepted 1 December 2008
Available online 6 December 2008

Keywords:
Electrocrystallization
Nucleation
Growth
Aluminum
Lead

ABSTRACT

Electrochemical deposition of aluminum and lead from basic molten $AlCl_3$–NaCl–KCl mixture on an aluminum electrode at 180 °C was studied by the methods of voltammetry, potential and current transient and constant current deposition. The deposition of aluminum was found to proceed via a nucleation/growth mechanism, while the deposition of lead was found to be diffusion controlled. The diffusion coefficient calculated for Pb^{2+} ions in basic melt by voltammetry was in agreement with the deductions of transient method. The analysis of the chronoamperograms indicates that the deposition process of lead on Al substrates was controlled by 3D diffusion control, nucleation and growth. The processes are manifested as peaks on a decaying chronoamperogram. Non-linear fitting methods were applied to obtain the kinetic parameters from the theoretical model proposed for this system. It is found that under more cathodic potential, the saturation number density of the formed lead nuclei and also the efficiency of the use of the available surface nucleation sites increased. The morphology of the aluminum deposits in both the presence and absence of $PbCl_2$ was examined by SEM.

1. Introduction

The electrocrystallization of metal on foreign substrates continues to attract a great deal of interest in modern electrochemistry due to its technological importance [1]. Nucleation and the growth of the first metallic nuclei formed on a substrate are critical steps that determine the physicochemical properties of electrodeposits and their studies are crucial in the understanding and control of the process. The first stage, the nucleation on a substrate surface, is in fact the important step in all metal deposition processes [2–7]. This early stage of electrochemical phase transformation is usually associated with a one, two- or three-dimensional nucleation process and the analysis of transients by means of different theoretical formalisms allows us to identify the different growth types or different steps which control or determine the nucleation processes [8–12]. The formation and growth of an electrodeposit involve complex nucleation processes and several models have been proposed to describe the cathodic deposition of metals especially when the substrate and the electrodeposit are the same [13,14]. It has also been shown that in many cases the electrolysis is mass transfer controlled and experiments have been devised to determine the diffusion coefficients of electroactive species [15].

In view of their interesting acid–base properties chloroaluminate melts (alkali metal chloride–$AlCl_3$ mixtures) have received considerable attention by molten salt chemists and a number of reports on the electrochemical and spectroscopic studies of both organic and inorganic species in this media have appeared in the literature [16].

The $AlCl_3$–NaCl melts have been employed as electrolytes for electrodeposition of metals and rechargeable batteries. During the charging of a rechargeable battery based on aluminum anodes, it has been found that [17,18] both aluminum dendrites and spongy deposits form under certain circumstances. As previously demonstrated [19], spongy deposits of aluminum could be prevented with the addition of $MnCl_2$ and codeposition of Al and Mn.

Amorphous alloys have received widespread attention because of their promising chemical, electrical, corrosion resistance and mechanical properties [20]. The effect of many inorganic additives in electrodeposition of aluminum from molten salts has been investigated. Among them $PbCl_2$ [20] and $SnCl_2$ [20,21] were found to have some beneficial effects on aluminum deposition.

Little work has been reported on voltammetry, chronopotentiometry and chronoamperometry studies in $AlCl_3$–NaCl–KCl melts. In our earlier work electrocrystallization of aluminum onto graphite from a molten electrolyte containing $AlCl_3$–NaCl–KCl was studied by the method of current transient and impedance spectroscopy [22,23]. In the early stage of the deposition and at low cathodic potentials, two-dimensional (2D) nucleation and layer-by-layer growth with some overlapping followed the initial double

---

* Corresponding author. Tel.: +98 21 22853551; fax: +98 21 22853650.
E-mail address: mjafarian@kntu.ac.ir (M. Jafarian).

0925-8388/$ – see front matter © 2008 Elsevier B.V. All rights reserved.
doi:10.1016/j.jallcom.2008.12.001

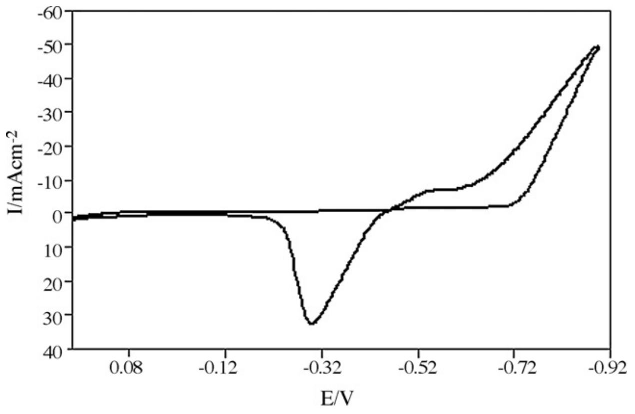

Fig. 1. Cyclic voltammogram of the aluminum electrode in basic molten salt (180 °C) without $PbCl_2$. The scan began at 0.2 V/Al with a scan rate of 60 mV s^{-1} and electrode area 0.5 cm^2.

layer charging. The processes manifested themselves as peaks on decaying chronoamperograms. In impedance spectroscopy investigations a model based on random birth and deterministic growth of monolayers was proposed, in which the edges were assumed to follow a propagation law. Parameters of impedance model in this system could be calculated from the fitting of experimental data to the faradaic impedance function derived theoretically.

It is the purpose of this study to investigate the electrochemical deposition of Al, Pb and Pb assisted Al on aluminum electrode from basic NaCl–KCl–$AlCl_3$ molten salt. This system can be of great significance from technological point of view because of its low vapor pressure and its low melting point of 115 °C. The kinetics of nucleation and growth of Pb on aluminum electrode is also studied by current transient.

2. Experimental

Materials used in this work were analytical grade of Merck origin. $AlCl_3$ was redistilled while NaCl and KCl were dried for 4 h at 400 °C prior to use. Fused electrolytes having the composition of 66–20–14 wt% ($AlCl_3$–NaCl–KCl) with the addition of 0.6% anhydrous $PbCl_2$ were employed. Handling of the materials and the procedures concerning the preparation of the fused electrolyte were much the same as reported previously [22]. The experiments were carried out at 180 °C.

The experiments were carried out in a conventional three-electrode cell with a hand polished aluminum rod with the surface area of 0.50 cm^2 forming the working electrode. Its potential was monitored against an aluminum (99.999% purity) reference electrode directly immersed in the melt [16]. A large graphite rod was used as the counter electrode.

The electrochemical cell was powered by an EG&G model 273A potentiostat/galvanostat run by a PC through M270 commercial software where the methods of cyclic voltammetry (CV), chronopotentiometry (CP) and chronoamperometry (CA) were employed. The data were analyzed through Statistica Stat Soft software. The surface morphology of the deposit was evaluated by scanning electron microscopy (SEM, Philips XL30).

3. Result and discussion

Cyclic voltammogram obtained in the potential range of 0.2 to −0.9 V/Al at 180 °C with the scan rate of 60 mV s^{-1} is presented in Fig. 1. In the cathodic half cycle, a significant crystallization overpotential is witnessed before aluminum electrodeposition begins. The electroactive entity, probably $AlCl_4^-$, starts to reduce at −0.73 V/Al. On reversing the potential sweep direction, nuclei already formed on the electrode surface continue to grow as a result of the $AlCl_4^- + 3e \leftrightarrow Al + 4Cl^-$ reaction remaining thermodynamically and kinetically favorable. The cross-over loop observed in reverse scan signifying nucleation/growth in the course of a cathodic scan [24] is accompanied by the anodic dissolution peak of Al at −0.3 V/Al. The high negative overpotential for deposition is largely due to the energy required to initiate nucleation while the negative on-set of stripping is traced to unstable structure of the deposit compared to more compact bulk Al. It was found that the cross-over potential is independent of the negative reverse potential. From these and the Fletcher [25,26] theory it is concluded that the growth rate is independent of the nucleation time (the experimental range of time selected for examining the growth of the nuclei). Therefore, the nuclei's growth rate is controlled by charge transfer and is determined only by the imposed potential.

The current step method is also a useful mean of detecting the presence of nucleation. Potential maxima at the beginning of the transition time can be attributed to the nucleation process [27]. Experimental chronopotentiograms exhibit a characteristic maximum in the early stages of deposition as shown in Fig. 2a. At the very beginning of the chronopotentiogram, the steep falling potential has contributions of both double layer as well as adsorptive pseudo capacitance charging [28] followed by monolayer deposition of the electroactive constituents. As the potential increases nucleation takes place [29] and overpotential is required to meet the galvanostatic conditions. As soon as nuclei are growing, the overpotential for reduction decreases. The product $I_o\tau^{1/2}$ was found to decrease with increasing applied current density, Fig. 2b, showing that the deposition of aluminum in basic melts is not controlled by diffusion and the reaction appears to be confined to the surface or near surface domains [30]. The decreasing trend suggests that a preceding chemical reaction mechanism similar to that observed in the $AlCl_3$–(Bupy)Cl electrolyte prevails [31].

A typical cyclic voltammogram of a $PbCl_2$ containing melt/aluminum electrode of a slightly basic nature at 180 °C is shown in Fig. 3. The scan rate was 60 mV s^{-1} in the potential range 0.1 to −0.9 V/Al. In the cathodic half cycle the on-set of the reduction peak at −0.5 V is clearly observed. Peak that appears at a −0.65 V is attributed to the reduction of Pb species. The peak current increases with scan rate and with $PbCl_2$ concentration. This peak is followed by the reduction of $AlCl_4^-$. No overcrossing was observed in the direct and reverse scans and the dissolution peak of deposited lead is observed at −0.12 V/Al. The relative locations of the deposition and stripping signals suggest complex irreversible type mechanism identified by Fletcher [25,26]. The ratio of the anodic peak current to the cathodic peak current obtained from this figure is nearly equal to one and also the columbic charge associated with the deposition process is nearly equal to that of the stripping process. This indicates that the deposited lead is an insoluble product with constant activity during the deposition and stripping process. A plot of peak current (i_p) *vs.* the square root

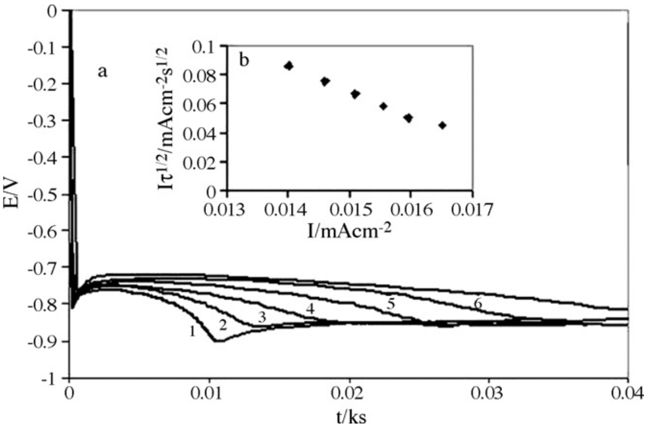

Fig. 2. (a) Chronopotentiogram of the aluminum electrode in basic melt without $PbCl_2$ in different current densities I_1 = 16.5 mA cm^{-2}, I_2 = 15.95 mA cm^{-2}, I_3 = 15.55 mA cm^{-2}, I_4 = 15.1 mA cm^{-2}, I_5 = 14.6 mA cm^{-2}, and I_6 = 14 mA cm^{-2}. (b) Plot of $I\tau^{1/2}$ *vs.* I for chronopotentiograms depicted in panel (a).

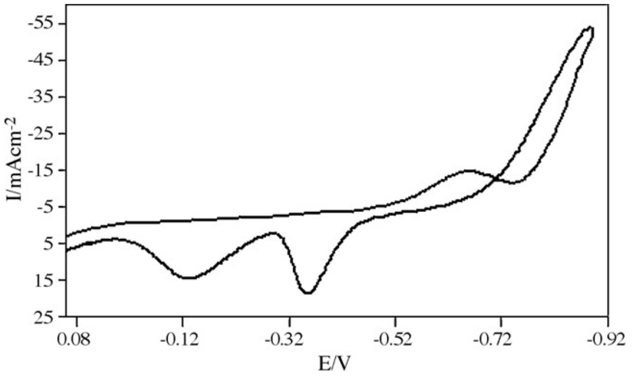

Fig. 3. Cyclic voltammogram of the aluminum electrode in basic melt in the presence of $PbCl_2$ (180 °C). The scan began at 0.1 V/Al with a scan rate of 60 mV s^{-1}.

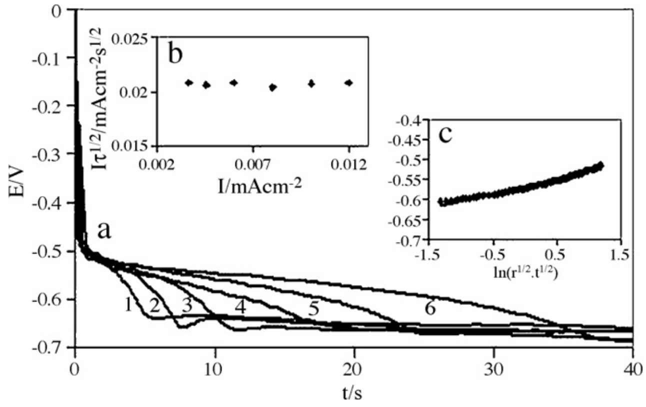

Fig. 5. (a) Chronopotentiogram of the aluminum electrode in basic melt in the presence of $PbCl_2$ (180 °C) in different current densities $I_1 = 12$ mA cm^{-2}, $I_2 = 10$ mA cm^{-2}, $I_3 = 8$ mA cm^{-2}, $I_4 = 6$ mA cm^{-2}, $I_5 = 4.5$ mA cm^{-2}, and $I_6 = 3.6$ mA cm^{-2}. (b) Plot of $I\tau^{1/2}$ *vs.* I for chronopotentiograms depicted in panel (a). (c) Dependence of E on $\ln(\tau^{1/2} - t^{1/2})$ derived in current density 4.5 mA cm^{-2}.

of scan rate (υ) for the deposition processes exhibits a straight line which passes through the origin within experimental error (Fig. 4). This feature point to the diffusion-controlled nature of lead deposition in molten salts and the corresponding dependency is well known ($I_p = 0.496n^{3/2}F^{3/2}C\alpha^{1/2}D^{1/2}\upsilon^{1/2}/R^{1/2}T^{1/2}$) [32]. From the slope of the straight line and using a transfer coefficient value of 0.5 [33,34], the diffusion coefficient of Pb^{2+} was obtained as $D_{Pb^{2+}} = 8 \times 10^{-6}$ cm^2 s^{-1}.

Chronopotentiometric measurements were also conducted with the aluminum electrode in slightly basic melt and in the presence of $PbCl_2$ and the results are presented in Fig. 5a where two steps appear in the chronopotentiograms. The first step is related to the reduction of ionic Pb species and is at a potential in agreement with that of the corresponding process in the cyclic voltammogram. The second step which appears at longer times is related to $AlCl_4^-$ reduction in basic melt. At the transition time, the potential rises sharply as the concentration of electroactive species at the electrode surface approaches zero. The product $I_o\tau^{1/2}$ was found to be constant with increasing current density, I_o, showing that Pb^{2+} reduction is controlled by diffusion and Sand's law is obeyed (Fig. 5b). The diffusion coefficient deduced from Sand's law is in very good agreement with that obtained in voltammetry and was found to be $D_{Pb^{2+}} = 8.5 \times 10^{-6}$ cm^2 s^{-1}. Logarithmic analysis of chronopotentiograms obtained in diffusion controlled region, Eq. (1), gave good linear fits for the insoluble product model where the plot of E *vs.* $\ln(\tau^{1/2} - t^{1/2})$ is linear (Fig. 5c). Assuming the value of α to be 0.5, from the slopes of these plots the average value of n was calculated to be 2 in agreement with expectations.

$$E = E_{th} + \frac{RT}{n\alpha F}\ \ln(\tau^{1/2} - t^{1/2}) \tag{1}$$

Fig. 6 presents chronoamperograms (CA) recorded at various applied cathodic potential steps in the range of −0.58 and −0.61 V in the presence of $PbCl_2$. As it can be seen, all transients are of the same shape with characteristic and well defined current maxima. Considering the shape of the experimental current transients, Scharifker et al. theory [35,36] was used for a 3D nucleation and growth mechanism limited by diffusion of the electroactive species (3D – *DC*) to evaluate further kinetic parameters.

In the curves shown in Fig. 6, the fast decaying current corresponding to the charging of the double layer is followed by a rising current due to the growth of the new phase and/or the increasing number of nuclei. At later stages the diffusion zones of adjacent nuclei overlap and the current density reaches a maximum followed by a decaying portion converging to a limiting current corresponding to the linear diffusion of the electroactive ions towards a planar electrode (Cottrell equation). The model of 3D nucleation with hemispherical diffusion control of the growing 3D clusters accounts for the kinetics of electrolytic phase formation in the early stages when diffusion of the depositing species from the bulk of the solution to the electrode/solution interface is the slow step. Eventually overlap of diffusion zones and the development of

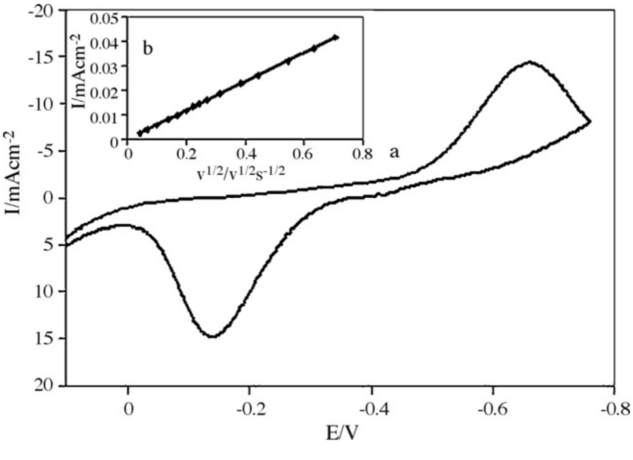

Fig. 4. (a) Cyclic voltammogram of the aluminum electrode in basic melt in limited potential range due to Pb deposition (180 °C). (b) The proportionality of cathodic peak currents to the square roots of sweep rate (2–500 mV s^{-1}).

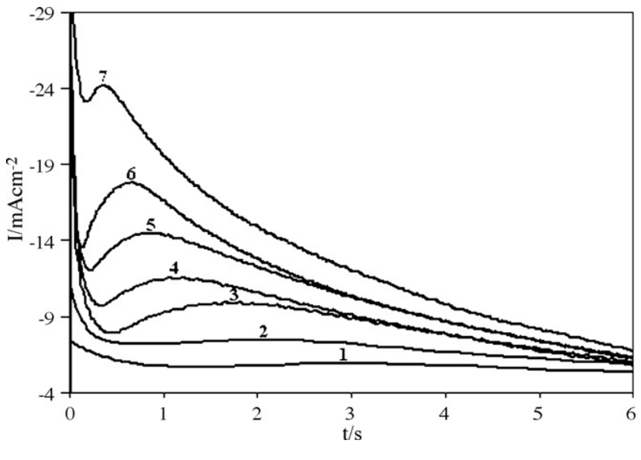

Fig. 6. Potentiostatic current transient obtained for deposition of Pb on aluminum at different potentials: (1) −0.58, (2) −0.585, (3) −0.59, (4) −0.595, (5) −0.6, (6) −0.605, and (7) −0.61 V/Al.

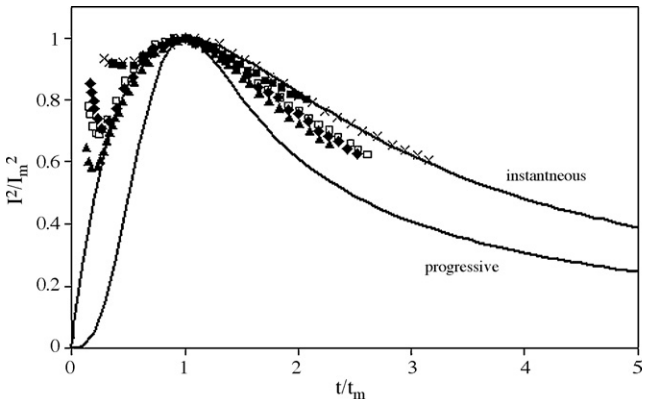

Fig. 7. Experimental and theoretical (—) current transients compared and presented in a non-dimensional I_2/I_m^2 *vs.* t/t_m, plot. Experimental current transients associated with the peak, recorded at −0.58 (×), −0.585 (■), −0.59 (□), −0.60 (♦), and −0.605 (▲) V/Al.

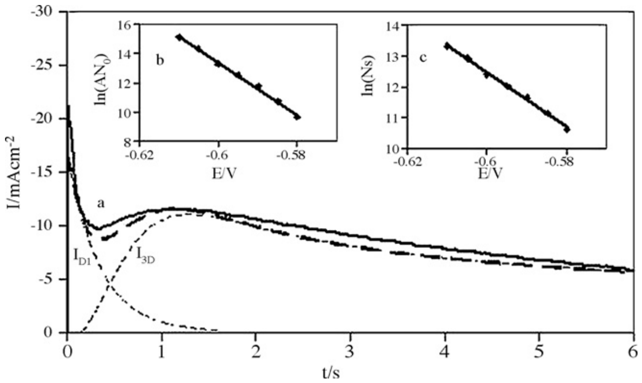

Fig. 8. (a) Experimental current transient (—) recorded at −0.595 V and a corresponding theoretical curve (- - -) for 3D nucleation transition. Contributions to the transient current from the double layer charging phenomenon (I_{DL}) and 3D diffusion control nucleation processes (I_{3D}) are also shown. (b) Plot of $\ln(AN_o)$ *vs.* E derived from theoretical current transient. (c) Dependence of $\ln(N_s)$ on E derived from theoretical current transient.

nucleation exclusion zones around the already established nuclei prevail. The time necessary to reach current maximum (t_m) depends on the overpotential and decreases as the potential is made more cathodic.

As a preliminary step all current transients were presented in a non-dimensional form, normalized current *vs.* time [$(I/I_m)^2$ *vs.* t/t_m] plots. I_m and t_m are the current and time values corresponding to the points of maxima used in the normalization processes [35]. According to this methodology a comparison of the theoretical plots with the experimental data allows the determination of nucleation process mechanism: instantaneous *vs.* progressive.

The current–time dependencies of the two types are distinctly different and follow Eqs. (2) and (3):

$$\frac{I^2}{I_m^2} = 1.9542\left(\frac{t}{t_m}\right)^{-1}\left\{1-\exp\left[-1.2564\left(\frac{t}{t_m}\right)\right]\right\}^2 \tag{2}$$

$$\frac{I^2}{I_m^2} = 1.2254\left(\frac{t}{t_m}\right)^{-1}\left\{1-\exp\left[-2.3367\left(\frac{t}{t_m}\right)^2\right]\right\}^2 \tag{3}$$

for instantaneous and progressive processes, respectively.

Fig. 7 shows such a non-dimensional plot for typical current transients recorded at different potentials for lead deposition on aluminum electrode. As it can be seen very clearly the relationship between the experimental curves and the theoretical models are the same in all potential. These curves indicate an instantaneous type of nucleation. At potentials greater than −0.625 V, nucleation tends to switch toward the progressive type for $t > t_m$.

In the case when the nucleation mechanism changes with the applied potential the evaluation of kinetic parameters based on the non-dimensional plots cannot be used. To estimate typical kinetic parameters for Pb deposition onto aluminum, we used Scharifker and Mostany's [37] general equation (Eq. (4)) for time evolution of the current density in the course of the 3D nucleation process limited by diffusion control growth (I_{3D-DC}).

$$I_{3D-DC} = \left(\frac{nFD^{1/2}C}{\pi^{1/2}t^{1/2}}\right)\left(1-\exp\left\{-N_o\pi kD\left[t-\frac{1-\exp(-At)}{A}\right]\right\}\right) \tag{4}$$

This equation is equally valid for describing instantaneous and progressive nucleation and does not require distinction of the nucleation mechanism prior to its use. In this equation zF is the molar charge transferred during electrodeposition, D is the diffusion coefficient, and C is the bulk concentration of the electroactive species. Time is t, the number density of active sites is N_o, the nucleation rate constant is A, and Eq. (5) defines k:

$$k = \left(\frac{8\pi CM}{\rho}\right)^{1/2} \tag{5}$$

M and ρ are the atomic weight and the density of the deposit, respectively.

As can be seen below, this expression can be presented in non-dimensional form which is in agreement with experimental data observed in Fig. 7.

$$\frac{I^2}{I_m^2} = \frac{t_m}{t}\frac{\{1-\exp[-xt/t_m+\alpha(1-\exp(-xt/\alpha t_m))]\}^2}{\{1-\exp[-x+\alpha(1-\exp(-x/\alpha))]\}^2} \tag{6}$$

$$x = N_o\pi Dkt_m$$

$$\alpha = \frac{N_o\pi Dk}{A}$$

The rate of nucleation does not remain constant during the electrocrystallization process but decreases continuously due to the decline of the number density of active site available for nucleation. Thus the saturation number density of the formed lead nuclei, N_s,

Table 1
Kinetic parameters obtained from the non-linear fitting of Eq. (4) with addition of double layer effect to the potentiostatic current transients shown in Fig. 6.

E (V *vs.* Ag/AgCl)	D ($\times10^6$ cm^2 s^{-1})	N_o ($\times10^{-5}$ cm^{-2})	A (s^{-1})	AN_o ($\times10^{-5}$ cm^{-2} s^{-1})	N_s ($\times10^{-5}$ cm^{-2})	N_s/N_o	$K_{1(DL)}$ (A cm^{-2})	$K_{2(DL)}$ (s^{-1})
−0.58	7.6	0.763	0.2	0.152	0.412	0.54	0.007	06
−0.585	8	1.186	0.4	0.474	0.702	0.592	0.011	1.2
−0.59	7.9	1.779	0.7	1.245	1.138	0.639	0.015	2.5
−0.595	8.1	2.262	1.2	2.715	1.64	0.725	0.0165	2.9
−0.6	8	2.866	2	5.733	2.4	0.837	0.017	3
−0.605	8	4.449	3.5	15.573	4.024	0.904	0.2	4.2
−0.61	8.2	6.18	6	37.083	6.043	0.977	0.033	4.5

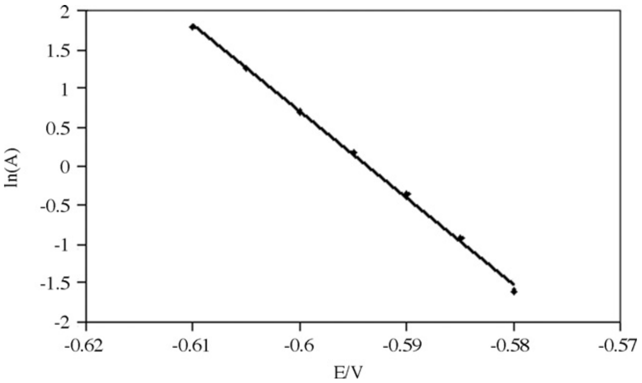

Fig. 9. Dependence of the nucleation rate on applied potential for the deposition of Pb.

is [35]:

$$N_s = \left(\frac{AN_o}{2kD}\right)^{1/2} \qquad (7)$$

Taking into account the contribution of double layer charging in current–time transient, $I_{DL} = k_1 \exp(-k_2 t)$, theoretical equations were fitted to the experimental current transient (Fig. 8a) and diffusion coefficient for ionic Pb species and characteristic kinetic parameters, the nucleation rate constant (A), number density of active sites (N_o), the AN_o product and the ratio N_s/N_o were obtained and are presented in Table 1.

As it was expected in accordance with the theory we found that A, N_o and N_s increase with the application of more cathodic electrode potential. The product AN_o which gives the stationary nucleation rate increased with increasing applied cathodic potential, Fig. 8b. The N_s/N_o ratio, which can also be defined as the efficiency of the use of the available surface nucleation sites, increases at more cathodic electrode potentials indicating that in more negative potentials higher number of surface sites are occupied by lead nuclei.

The potential dependence of $\ln(N_s)$ is linear pointing to the exponential relationship between N_s and the electrode potential, Fig. 8c. The potential dependence of N_o is due to distributed energies of nucleation on different sites. At low overpotentials, nucleation is restricted to very few active sites on the surface which become exhausted at an early stage in the process and nucleation thus approaches the instantaneous limit at low supersaturation. At very high cathodic overpotential the nucleation approaches progressive limit (Fig. 9).

Within the framework of the atomistic theory of nucleation [38], the number of atoms necessary to form the critical nucleus can be estimated directly from the potential dependence of the nucleation rate. The largest cluster for which the probability for attachment of one atom is less than one-half is defined as critical. The attachment of a new atom converts this cluster into a stable one for which the probability for attachment of the next atom is already higher than one-half and henceforth able to grow spontaneously. According to the atomistic theory, the nucleation rate can then be expressed as

$$A = K_1 \exp\left(\frac{-W_k}{kT}\right) \exp\left(\frac{\alpha n e_o E}{kT}\right) \qquad (8)$$

where K_1 is the pre-exponential factor, e_o is the elementary electric charge, α is the cathodic transfer coefficient, E is the overpotential, and W_k is the reversible work for the formation of a critical nucleus consisting of N_k atoms. It has been shown [39] that, regardless of the nucleation model and for the case when the excess Gibbs energy of nucleus formation is potential dependent, N_k, A, and E are related through

$$N_k = \frac{kT}{ne_o}\left(\frac{d\ \ln A}{dE}\right) - \alpha \qquad (9)$$

Eq. (9) indicates that the slope of an experimental curve of ln A *vs.* E gives the size of the critical nucleus. The experimental ln A *vs.* potential plots for all concentrations studied in this work gave straight lines throughout the potential range. From their slope at 453 K and using a transfer coefficient value of 0.5, Eq. (9) the number of atoms that form critical nucleus was estimated to be 2.1 atoms.

3.1. Constant current deposition studies

Fig. 10a presents the scanning electron micrographs of Al electrodeposited from basic melt on aluminum electrode in current density 0.06 A cm^{-2}. As can be seen, in basic melts at 180 °C, it seems that dull, dark, spongy deposits and weakly adherent to the substrate are always formed on. Fig. 10b presents the scanning electron micrographs electrodeposited surface from basic melt with addition of $PbCl_2$ on aluminum electrode in current density 0.06 A cm^{-2}. In the presence of $PbCl_2$ the Al layer was silver bright, partly compact, and smoother. When $PbCl_2$ is present, codeposition of Al and Pb apparently promotes the nucleation [19] and therefore the formations of spongy deposits are avoided.

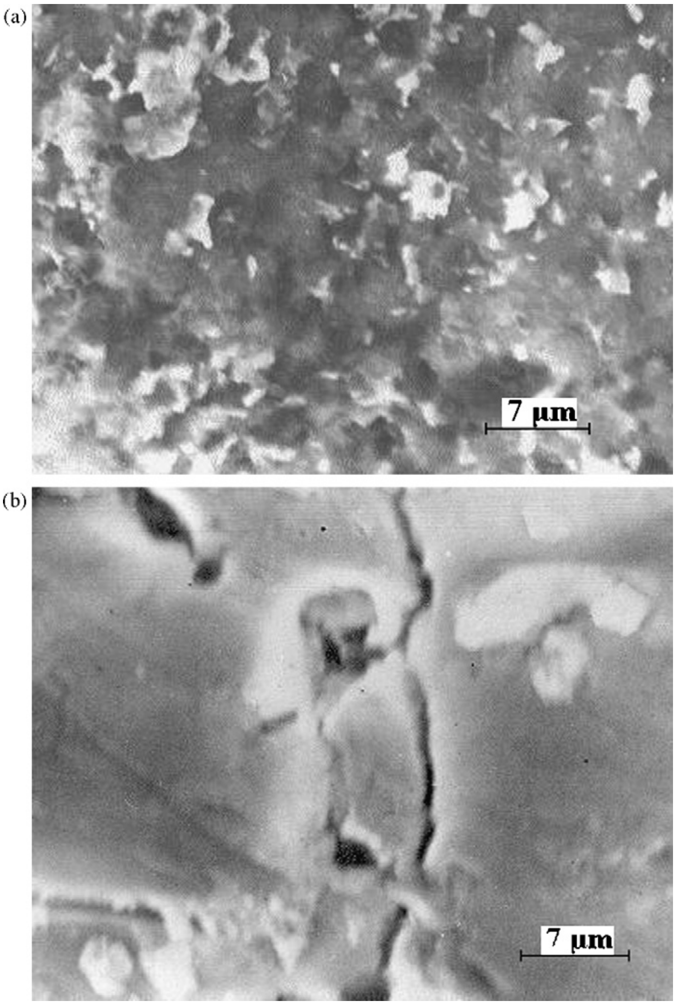

Fig. 10. (a) Surface of aluminum deposited in basic melt by SEM micrograph. (b) Surface of aluminum deposited in basic melt in the presence of 0.6% $PbCl_2$ by SEM micrograph. Current density 0.06 A cm^{-2}, deposition time 8 h, temperature 180 °C, and melt composition 66–20–14 wt%.

4. Conclusion

Electrodeposition of aluminum and lead onto an aluminum electrode from molten ($AlCl_3$–NaCl–KCl) salts were studied by the methods of cyclic voltammetry, chronopotentiometry and chronoamperometry. Electrochemical deposition of aluminum onto aluminum electrode in basic melt was found to proceed via a nucleation/growth mechanism, while deposition of lead from basic melts showed that ionic Pb species reduction was controlled by diffusion. The diffusion coefficient of such species was obtained by voltammetry, chronopotentiometry and is in agreement with the chronoamperometric measurements and was found to be 8×1^{-6} $cm^2\,s^{-1}$.

The analyses of the chronoamerograms indicate that the deposition process of lead on Al substrates is 3D nucleation and growth which controlled by diffusion. The magnitudes of the associated kinetic parameters and the parameter reflecting double layer charging in the initial stages of deposition are reported. The kinetic parameters of the electrocrystallization of lead increase with increasing applied potential. The efficiency of the utilization of the available surface nucleation sites in different potentials indicates that in more cathodic potential larger number of surface sites are occupied with lead nuclei. On the basis of atomistic theory the number of atoms that form a critical nucleus was found to be 2.1. In basic solutions the deposit morphology is dull grey, spongy and non-compact while in the presence of $PbCl_2$ smoother and non-porous aluminum is formed.

References

[1] H.A. Hjuler, R.W. Berg, N.J. Bjerrum, J. Power Sources 10 (1985) 1–11.
[2] R. Beratazzoli, D. Pletcher, Electrochim. Acta 38 (1993) 671–676.
[3] E. Gomez, M. Marin, F. Sanz, E. Valles, J. Electroanal. Chem. 422 (1997) 139–147.
[4] M.S. Cruz, F. Alanzo, J.M. Palacois, J. Appl. Electrochem. 23 (1993) 364–370.
[5] M. Jafarian, M.G. Mahjani, F. Gobal, I. Danaee, J. Appl. Electrochem. 36 (2006) 1169–1173.
[6] E. Souteyrard, G. Maruin, D. Merciner, J. Electroanal. Chem. 161 (1984) 17–30.
[7] G. Gunawardena, G. Hills, I. Montenegro, B. Scharifker, J. Electrochem. Soc. 138 (1982) 225–231.
[8] D.J. Astely, J.A. Harrison, H.R. Thirsk, Trans. Faraday Soc. 64 (1968) 192–201.
[9] M. Fleischmann, H.R. Thirsk, Electrochim. Acta 2 (1960) 22–49.
[10] G.A. Gunawardena, G.J. Hills, I. Montenegro, Electrochim. Acta 23 (1978) 693–697.
[11] M. Fleischmann, H.R. Thirsk, in: P. Delahay (Ed.), Advanced Electrochemistry and Electrochemical Engineering, vol. 3, Academic Press, New York, 1963, p. 123.
[12] I.N. Stranski, R. Kaishev, Z. Physik 36 (1935) 393–398.
[13] M. Volmer, Z. Physik 22 (1921) 646–652.
[14] W. Kautek, S. Birkle, Electrochim. Acta 34 (1989) 1213–1218.
[15] K. Kawamura, Electrochim. Acta 12 (1967) 1233–1244.
[16] M. Paucirova, K. Matiasovsky, Electrodep. Surf. Treat. 3 (1975) 121–128.
[17] L. Qingfeng, H.A. Hjuler, R.W. Berg, N.J. Bjerrum, J. Electrochem. Soc. 138 (1991) 763–766.
[18] P. Rolland, G.J. Mamantov, J. Electrochem. Soc. 123 (1976) 1299–1303.
[19] L. Qingfeng, H.A. Hjuler, R.W. Berg, N.J. Bjerrum, J. Electrochem. Soc. 137 (1990) 2794–2798.
[20] K. Grjotheim, K. Mathiasovsky, Acta Chem. Scand. A 34 (1980) 666–670.
[21] N. Koura, J. Electrochem. Soc. 127 (1980) 1529–1531.
[22] M. Jafarian, M.G. Mahjani, F. Gobal, I. Danaee, J. Electroanal. Chem. 588 (2006) 190–196.
[23] M. Jafarian, F. Gobal, I. Danaee, M.G. Mahjani, Electrochim. Acta 52 (2007) 5437–5443.
[24] R. Greef, R. Peat, L.M. Peter, D. Pletcher, J. Robinson, Instrumental Methods in Electrochemistry, Ellis Horwood, Chichester, 1985 (Chapter 9).
[25] S. Fletcher, C.S. Halliday, D. Gates, M. Westcott, T. Lwin, G. Nelson, J. Electroanal. Chem. 159 (1983) 267–285.
[26] S. Fletcher, Electrochim. Acta 28 (1983) 917–923.
[27] D.J. Hills, D.J. Schriffrin, J. Thomson, Electrochim. Acta 19 (1974) 657–670.
[28] F. Lantelme, J. Chevalet, J. Electroanal. Chem. 121 (1981) 311–327.
[29] G. Gunawardena, G. Hills, I. Montenegro, B. Scharifker, J. Electroanal. Chem. 138 (1982) 225–239.
[30] G.R. Stafford, G.M. Haarberg, Plasma Ions 2 (1999) 35–44.
[31] Q.-X. Qin, M. Skyllas-Kazacos, J. Electroanal. Chem. 168 (1984) 193–206.
[32] A.J. Bard, L.R. Faulkner, Electrochemical Methods: Fundamentals and Applications, second ed., Wiley, 2000.
[33] L. Komsiyska, G. Staikov, Electrochim. Acta 54 (2008) 168–172.
[34] G. Baltrunas, A. Valiuniene, Z. Margarian, G. Viselgiene, G. Popkirov, Electrochim. Acta 53 (2008) 6513–6520.
[35] B.R. Scharifker, G. Hills, Electrochim. Acta 28 (1983) 879–889.
[36] M. Miranda-Hernandez, I. Gonzalez, N. Batina, J. Phys. Chem. B 105 (2001) 4214–4223.
[37] B.R. Scharifker, J. Mostany, J. Electroanal. Chem. 177 (1984) 13–23.
[38] A. Milchev, S. Stoyanov, R. Kaichev, Thin Solid Films 22 (1974) 267–274.
[39] D. Kaschiev, J. Chem. Phys. 76 (1982) 5098–5102.